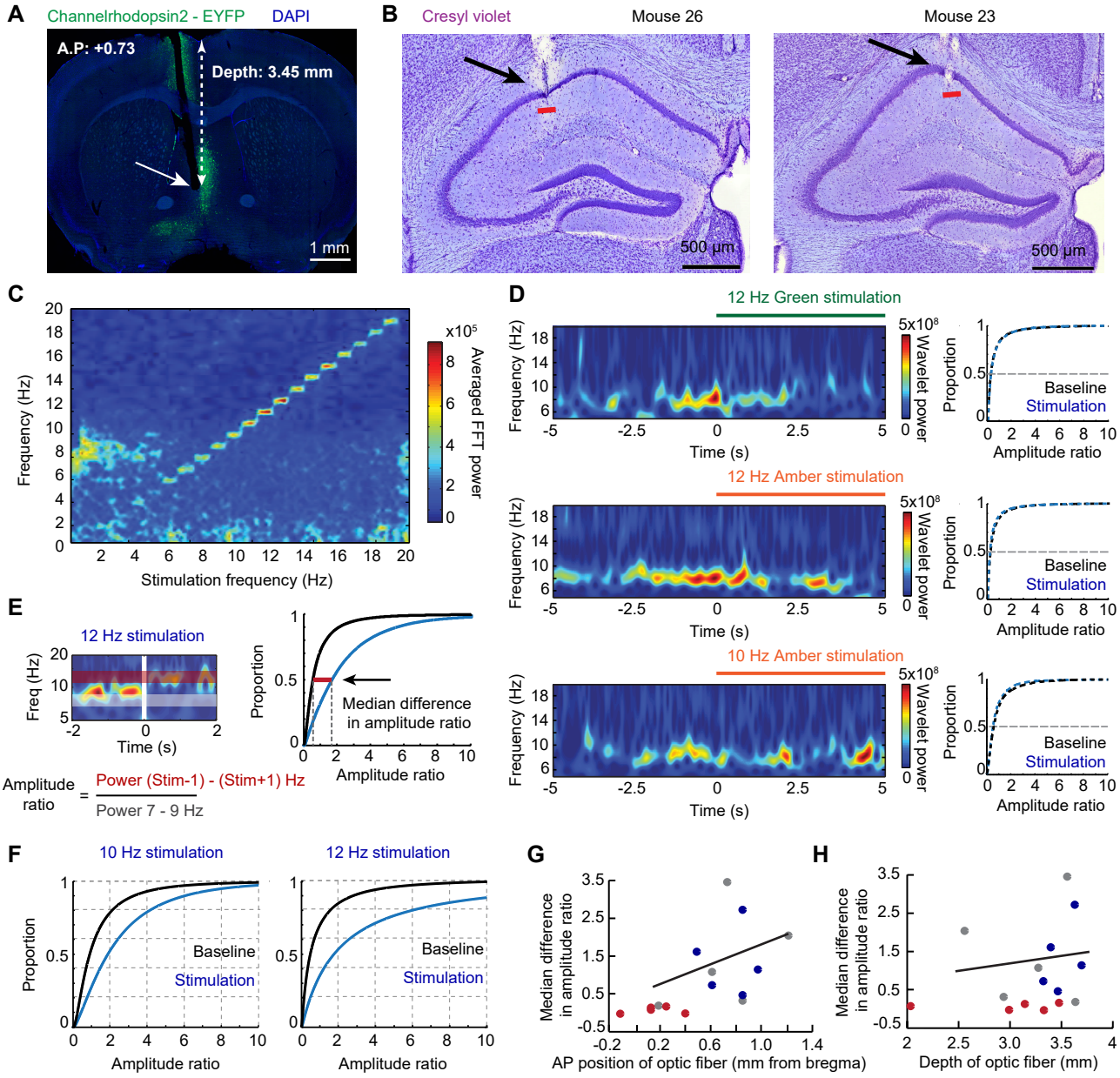

Figure S1. Histology of viral-induced expression, tetrode recording locations and quantification of pacing efficiency. Related to Figure 1.

(**A**) Representative coronal section through the MSA with the end of the optic fiber track marked by a *white arrow*. The depth of the optic fiber (*stippled white line*) was measured for each animal. (**B**) Tetrode recording tracks for two representative mice. All tracks were confirmed to terminate in the dorsal CA1 region. *Black arrows* point to the tetrode track in the hippocampus and *red lines* demarcate the final position of the tetrode tip. (**C**) Optogenetic pacing is effective across a broad range of frequencies. Optogenetic stimulation was performed on the rectangle track in 1 Hz steps (from 1-20 Hz) for a duration of 5 seconds per step. The color-coded frequency spectrum demonstrates a near one-to-one relation between stimulation frequencies >6 Hz and LFP frequencies, but endogenous theta frequency was predominant during stimulation at lower frequencies. (**D**) Green and amber laser stimulation was used to control for the possibility that light stimulation would exert unspecific control over hippocampal theta oscillations. *Left*: Wavelet spectrograms of green and amber light stimulation confirm a lack of hippocampal theta pacing. *Right*: Amplitude ratios did not differ between baseline and stimulation with green or amber light. (**E**) Schematic depicting the calculation of the amplitude ratio. Using the wavelet- based power, the ratio between the endogenous band (*violet stripe*, 7-9 Hz) and the stimulation band (*red stripe,* 11-13 Hz for 12 Hz stimulation) was calculated on a moment by moment basis for stimulation (*blue line*) and no stimulation (*black line*) periods. The *red bar* that is highlighted by the *black arrow* denotes the difference in the median amplitude ratio between no-stimulation and stimulation periods. (**F**) CDF plots highlight that amplitude ratios were substantially increased during optogenetic stimulation at 10 Hz and 12 Hz across all mice combined. (**G**) Scatter plot of the anteroposterior (AP) position of the optic fiber (from bregma) and the pacing efficiency for each animal. *Blue dots* correspond to the mice that were used for single unit analyses, and *red dots* were the mice with low virus expression, which were not included in the correlation analysis because pacing would not be expected in these mice for any fiber position. (**H**) Scatter plot of the depth of the optic fiber (from brain surface) and the pacing efficiency for each animal. *Blue dots* and *red dots* as in G.

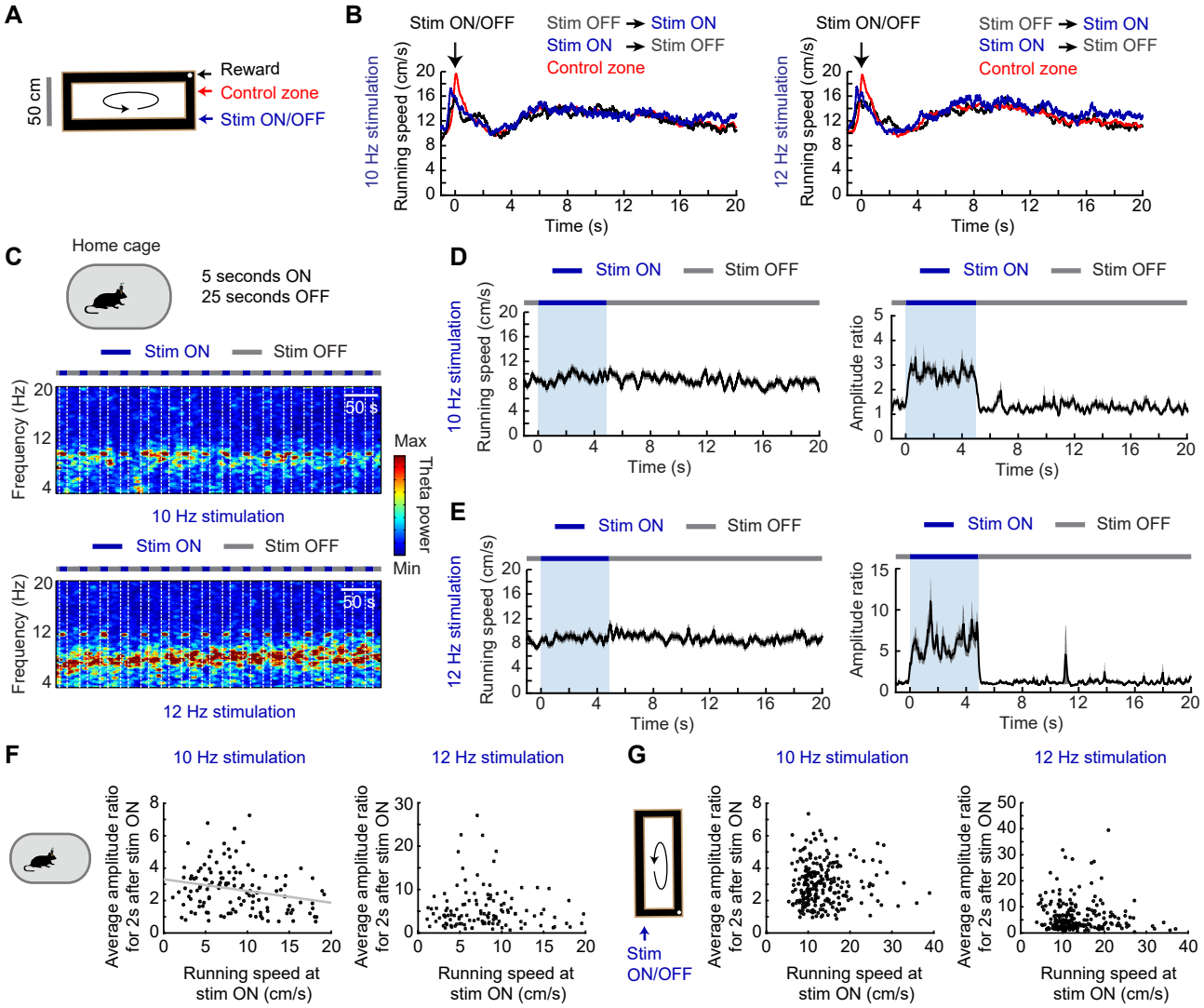

Figure S2. Effects of optogenetic stimulation of MSA PV neurons on running speed and theta oscillations. Related to Figure 2.

(**A**) Schematic of the circular track used for behavior. Animals were trained to run around the track to obtain a reward in one corner, while light stimulation was turned on or off at the marked site on every other lap. *Black arrow* shows the direction of running. The site that is demarcated by the *red arrow* (control zone) was used for analysis shown as a *red line* in (B). (**B**) Running speed over time is shown for laps when the stimulation was turned on (*blue*) and laps when the stimulation was turned off (*black*) across all mice. In both cases, there was an apparent increase in running speed when the light turned on/off (time 0). To test whether the increase resulted from the requirement that the animal always had to be moving across a boundary for the laser status to change, we selected an arbitrary boundary along the track (control zone in A) and calculated the running speed relative to the time when the animal crossed into the control zone. An apparent increase in running speed was found even in this case, confirming that the observed changes in running speed emerged from the criterion that movement across a boundary was required to change the laser status. (**C**) Because behavior on the track required a contingency for laser stimulation to turn on (i.e., crossing a boundary), we also performed recordings in the home cage with optical stimulation at fixed intervals (5 s ON, 25 s OFF). As for the track, example spectrograms of recordings in the home cage show that the LFP power shifted to the stimulation frequency during this paradigm. (**D, E**) *Left*, Average running speed aligned to the 5-s light stimulation at 10 Hz and 12 Hz. There was no change in the running speed upon light onset (*blue*, light on period). *Right*, Average amplitude ratio aligned to the 5-s light stimulation at 10 Hz and 12 Hz. Onset of rhythmic optical stimulation led to a rapid and reversible shift of the LFP frequency. (**F**) Scatter plot of the amplitude ratio versus running speed at stimulation onset during recordings in the home cage (Spearman rank correlation, 10 Hz stimulation: n = 127 stimulation onsets, R = -0.25, $p = 0.005$; 12 Hz stimulation: n = 125 stimulation onsets, R = -0.025, $p = 0.78$). (**G**) Scatter plot of the amplitude ratio versus running speed at stimulation onset during recordings on the track (Spearman rank correlation, 10 Hz stimulation: n = 241 stimulation onsets, R = 0.011, $p = 0.86$; 12 Hz stimulation: n = 226 stimulation onsets, R = -0.047, $p = 0.48$).

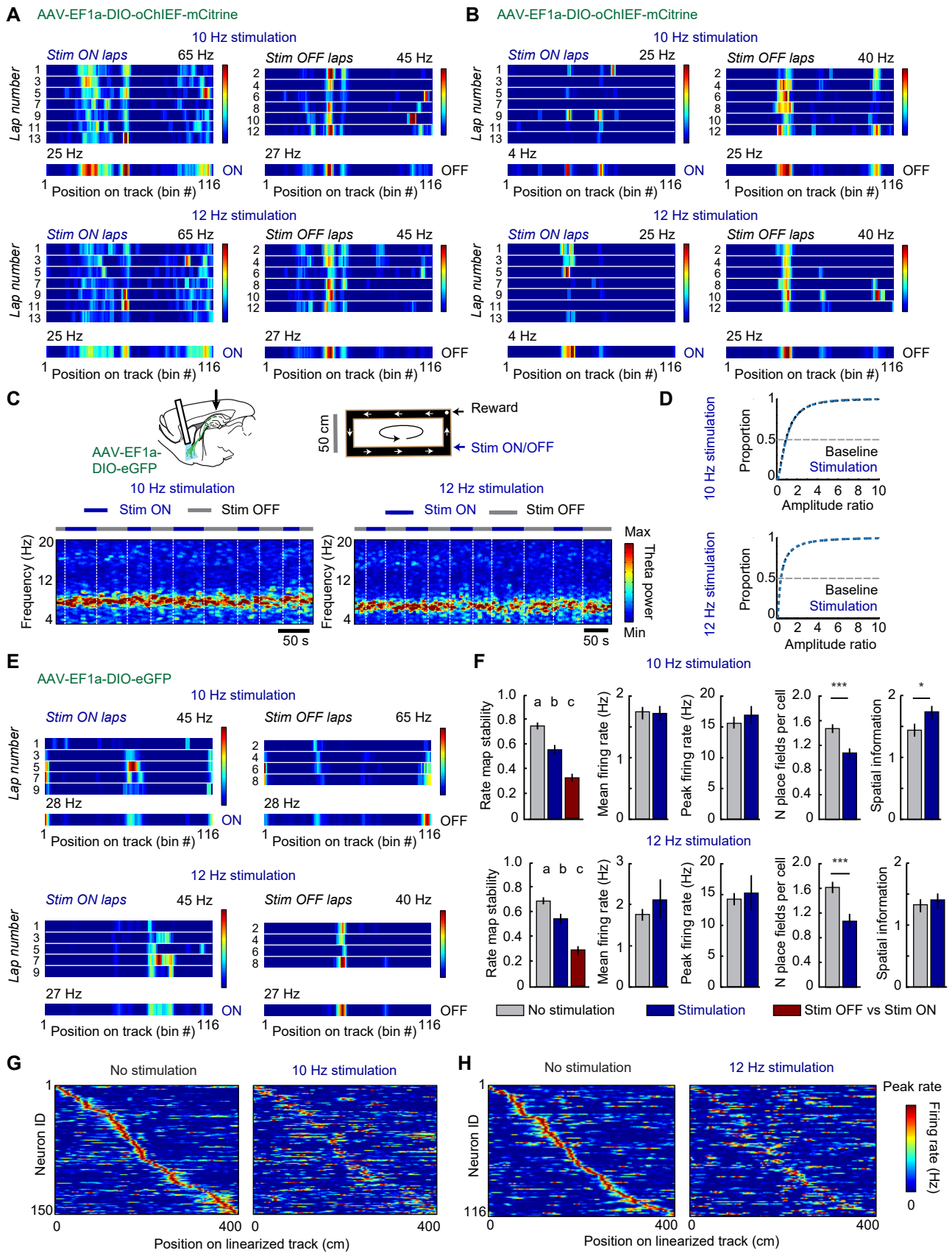
A
AAV-EF1a-DIO-oChIEF-mCitrine
10 Hz stimulation
Stim ON laps
65 Hz
Stim OFF laps
45 Hz
Lap number
25 Hz
27 Hz
ON
OFF
Position on track (bin #)
12 Hz stimulation
B
AAV-EF1a-DIO-oChIEF-mCitrine
10 Hz stimulation
Stim ON laps
25 Hz
Stim OFF laps
40 Hz
4 Hz
25 Hz
12 Hz stimulation
C
AAV-EF1a-DIO-eGFP
50 cm
Reward
Stim ON/OFF
10 Hz stimulation
12 Hz stimulation
Stim ON
Stim OFF
Frequency (Hz)
Max
Theta power
Min
50 s
D
10 Hz stimulation
12 Hz stimulation
Proportion
Baseline
Stimulation
Amplitude ratio
E
AAV-EF1a-DIO-eGFP
10 Hz stimulation
Stim ON laps
45 Hz
Stim OFF laps
65 Hz
28 Hz
12 Hz stimulation
40 Hz
27 Hz
F
10 Hz stimulation
12 Hz stimulation
Rate map stability
Mean firing rate (Hz)
Peak firing rate (Hz)
N place fields per cell
Spatial information
a b c
***
*
No stimulation
Stimulation
Stim OFF vs Stim ON
G
No stimulation
10 Hz stimulation
Neuron ID
Position on linearized track (cm)
H
No stimulation
12 Hz stimulation
Peak rate
Firing rate (Hz)

Figure S3. Place cells were reversibly reorganized in response to blue light stimulation in mice with septal oChIEF expression and in GFP controls. Related to Figure 3.

(**A, B**) Examples of place cells that were recorded during both 10 Hz and 12 Hz stimulation sessions from oChIEF injected mice. The cells reorganized reversibly and similarly during stimulation compared to no stimulation, regardless of the stimulation frequency. Each subplot shows a lap-by-lap linearized rate map for the cell during light-on and light-off conditions with the average linearized rate map across all trials in the same condition on the bottom. The peak rate of the color scale to the right is provided on top of the plots. (**C**) The recording paradigm used for the 3 mice injected with a Cre-dependent virus expressing GFP was identical to the paradigm used for mice with oChIEF expression. As expected for GFP expression, the spectrogram depicts no change in the LFP frequency during light stimulation at either 10 Hz or 12 Hz. (**D**) CDF plots show that there was no change in the amplitude ratio between no stimulation and stimulation sessions for GFP control mice. The curves overlap so precisely that they are difficult to disambiguate. (**E**) Example place cells show a reversible reorganization of their spatial fields in response to 10 Hz and 12 Hz stimulation in the control mice, suggesting that place field remapping is independent of changes in theta oscillations. (**F**) The firing properties of place cells (rate map stability, mean firing rate, peak firing rate, number of place fields per cell, and spatial information) were affected similarly during light stimulation in GFP mice as during light stimulation in oChIEF mice (also see **Fig. 3**), suggesting that partial remapping was sensory-driven by the visibility of blue light during stimulation periods (Repeated measures one way ANOVA, rate map stability, 10 Hz: n = 99 cells, $F(1.868, 183.1) = 64.49$, $p < 0.0001$; 12 Hz: n = 90 cells, $F(1.992, 173.3) = 57.2$, $p < 0.0001$; Wilcoxon matched pairs signed rank test, 10 Hz, mean firing rate: $p = 0.147$; peak firing rate: $p = 0.825$; number of fields: $p = 0.0002$; spatial information: $p = 0.013$; 12 Hz: mean firing rate: $p = 0.369$; peak firing rate: $p = 0.258$; number of fields: $p = 0.0002$; spatial information: $p = 0.725$). Histograms depict mean ± SEM. (**G, H**) Linearized firing rate maps for all cells that were recorded during no-stimulation and stimulation laps from the oChIEF injected mice. While cells were reordered separately for the no-stimulation and stimulation condition in **Fig. 3F**, the cells are ordered here by their position on the track in the no-stimulation laps, and the same order was maintained for the stimulation laps.

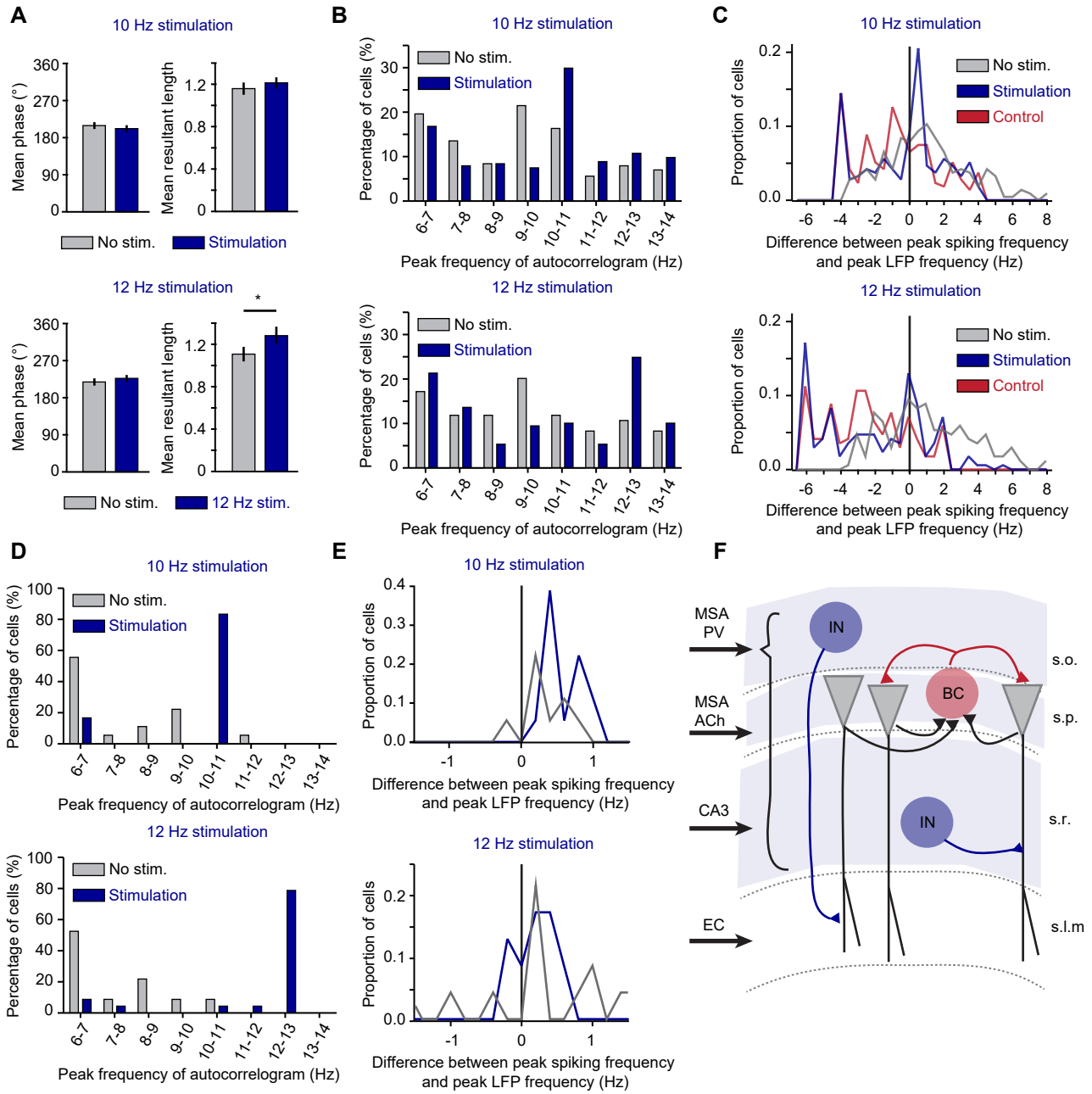

Figure S4. Theta phase and theta frequency spiking properties of CA1 principal cells and interneurons during optogenetic pacing of MSA PV neurons. Related to Figure 4.

(**A**) The mean phase and mean resultant length of spiking at theta frequencies did not differ between no-stimulation and 10 Hz-stimulation laps. During 12 Hz-stimulation laps, there was a minor increase in the mean resultant length, while the mean phase was not different. (**B**) Histograms depicting the distribution of peak frequencies (in the 6-14 Hz range) of CA1 principal cell spiking during no-stimulation versus stimulation laps. Without stimulation, there was an over-representation of frequencies above the endogenous theta frequency. During stimulation, the most common frequency was above the stimulation frequency. Note that low theta rhythmicity often results in the detection of a peak at the lower boundary of our detection range (i.e., 6-7 Hz). (**C**) Probability distribution of the difference between the peak frequency of CA1 pyramidal cell spiking (measured from the autocorrelogram of each cell) and the peak LFP frequency. (**D**) Same as B, but for CA1 interneuron spiking. Most interneurons accelerated their frequency compared to the stimulation frequency. (**E**) Same as C, but for CA1 interneurons. Most cells fired ~0.5-1 Hz faster than the ongoing LFP frequency during stimulation trials. Also see **Fig. 4E**. (**F**) Schematic of projections from the MSA to the hippocampal CA1 area. While cholinergic projections from the MSA terminate in the vicinity of the pyramidal cell layer, GABAergic septal neurons are known to project broadly throughout stratum oriens (s.o.), stratum pyramidale (s.p.), and stratum radiatum (s.r.) and are known to terminate on various interneuron subtypes, including those that preferentially target dendritic regions[S1-S4]. Septal control over rhythmic synaptic activity in the dendritic regions while the oscillation frequency of CA1 cells is controlled by feedback circuits between principal cells could explain the direct control of the LFP frequency by septal stimulation while the cellular oscillation frequency is simultaneously accelerated. *MSA*, medial septal area; *EC*, entorhinal cortex; *IN,* interneuron; *BC*, basket cell; *ACh*, Acetylcholine; *PV*, Parvalbumin; s.*o.*, stratum oriens; *s.p.*, stratum pyramidale; *s.r.*, stratum radiatum; *s.l.m.*, stratum lacunosum-moleculare.

SUPPLEMENTAL REFERENCES

S1. Joshi, A., Salib, M., Viney, T.J., Dupret, D., and Somogyi, P. (2017). Behavior-Dependent Activity and Synaptic Organization of Septo-hippocampal GABAergic Neurons Selectively Targeting the Hippocampal CA3 Area. Neuron *96*, 1342-1357 e1345.

S2. Freund, T.F., and Antal, M. (1988). GABA-containing neurons in the septum control inhibitory interneurons in the hippocampus. Nature *336*, 170-173.

S3. Unal, G., Joshi, A., Viney, T.J., Kis, V., and Somogyi, P. (2015). Synaptic Targets of Medial Septal Projections in the Hippocampus and Extrahippocampal Cortices of the Mouse. J Neurosci *35*, 15812-15826.

S4. Frotscher, M., and Leranth, C. (1985). Cholinergic innervation of the rat hippocampus as revealed by choline acetyltransferase immunocytochemistry: a combined light and electron microscopic study. J Comp Neurol *239*, 237-246.